

# Effects of internal-phase contents on porous polymers prepared by a high-internal-phase emulsion method

Wang-Fa Xu · Rui Bai · Fa-Ai Zhang

Received: 27 January 2014 / Accepted: 7 July 2014 / Published online: 19 August 2014  
© Springer Science+Business Media Dordrecht 2014

**Abstract** A series of porous polymers poly(styrene-divinylbenzene) was synthesized by the polymerization of 9 : 1 (v/v) styrene/divinylbenzene using high-internal-phase emulsions (HIPEs) as template, cetyltrimethyl ammonium bromide as a surfactant in the presence of water-miscible organic additives ethanol, with internal-phase contents varied from 82.5 to 94.0 %. The effects of the internal-phase contents on the microstructure of the resulting polymers were characterized by scanning electron microscopy and mercury intrusion porosimeter. The apparent density, compressive strength, water and toluene absorption and release behavior of the polymers with different porosity were investigated. The results showed that the properties of the porous polymer were significantly influenced by the internal-phase content. The increase in the internal-phase content increased the pore volume, thus increased the water and toluene absorption values, but decreased the apparent densities and the compressive strength of the porous polymers. The highest water and toluene absorption values were found for the sample prepared with the highest internal-phase content (94.0 %), which reached 11.65 and 21.64 cm<sup>3</sup>/g (based on the weight of the porous polymer), respectively. The water and toluene absorption kinetics of the porous polymers were well described by a pseudo-second-order kinetic model. The toluene release rates of the porous polymers were increased with the increased internal-phase content.

**Keyword** Porous polymer · High-internal-phase emulsion · Absorption · High-internal-phase-content · Kinetics

W.-F. Xu · R. Bai · F.-A. Zhang (✉)  
College of Material Science and Engineering, Guilin University of Technology, No 12 Jiangan Road, Guilin 541004, People's Republic of China  
e-mail: zhangfaai@163.com

## Introduction

Porous materials are attracting considerable attention because of their high surface areas and physicochemical properties [1, 2]. As a kind of the porous material, porous polymers are extensively applied as microreactors, ion-exchange resins, molecular recognition devices, fuel and petroleum recovery devices, fuel cell membranes, electrode materials for batteries, gas storage devices, etc. [3–5]. The traditional methods of preparing porous polymer are categorized as hard or soft-template methods [4], both of which cannot control the pore size and pore size distribution. Lately, high-internal-phase emulsions (HIPEs) are used as templates to regulate the pore size and pore size distribution of porous polymers [6–11]. HIPEs, also known as high-concentration emulsions, contain a discontinuous phase with a volume fraction >74 %. In some systems, the volume fraction even reaches 99 % [7, 12]. Generally, the discontinuous phase (aqueous phase) comprises a solvent and an initiator that does not dissolve in the monomer, while the continuous phase (oil phase) composes a monomer (with the appropriate crosslinking monomer) and an emulsifier. After polymerization and drying, porous polymers with specific pore size and pore size distribution can be obtained. Porous polymers prepared by the HIPE method are named polyHIPE [6, 13–18]. Given that polymerization occurs around the droplets of the internal phase, the pore content of polyHIPE can reach 99 %. The microstructures of polyHIPE can also be controlled by regulating the internal-phase content [1, 19]. PolyHIPEs with a specific surface area more than 700 m<sup>2</sup>/g (Brunauer-Emmett-Teller method) can be produced by adjusting the monomer composition, addition method, or the amounts of initiator and emulsifier. The droplet size of the internal phase can be adjusted in HIPEs and used to synthesize various porous materials with pore sizes ranging from 10 to 100 μm. Based on the unique microstructure properties of the polyHIPE, they are widely used in the fields

of microreactor manufacture [20], tissue engineering [6, 21] and selective absorption [22, 23], and capillary electrochromatography [24].

The main factors influencing the stability of HIPEs and the microstructure of polyHIPEs are internal-phase content [17, 19, 25–27] and surfactants [7, 8, 16, 28]. The effects of emulsion preparation conditions, such as stirring speed and rate of aqueous droplet-phase addition, on the foam microstructure and properties of porous polymers have been investigated [19, 27]. However, most researcher have used nonionic surfactants or mixtures of nonionic and ionic surfactants. Chen used the cationic cetyltrimethyl ammonium bromide (CTAB) as a sole surfactant to stabilize HIPEs [7]. They synthesized open, porous emulsion-templated monoliths with a significantly high pore volume ( $14.7 \text{ cm}^3/\text{g}$ ), as well as uniform pore diameters and cell sizes [29]. They added ethanol or poly(ethylene glycol) as water-miscible organic additives to tailor the morphology of the system [7], and found that the interconnect diameters gradually increased with the increased ethanol concentration from 1.0 to 5.0 wt %, and 8.0 wt % [7]. However, studies of using CTAB as a surfactant on the microstructure and the properties of the polyHIPE are rare. It is well known that the microstructures of polyHIPE significantly may influence the properties of polyHIPEs [25]. In the present work, a series of porous polymers was synthesized by a HIPE method using CTAB as a surfactant in the presence of ethanol. The effects of the internal-phase content on the HIPEs and polyHIPEs were discussed. The apparent density, mechanical properties, and maximum water and toluene absorption values of the polyHIPE were also investigated.

## Experimental

### Materials

Styrene [St, Chemical Pure (CP)], cetyltrimethyl ammonium bromide [CTAB, analytical reagent (AR)], ammonium persulfate (APS, AR) were purchased from Xilong Chemical Plant in Shantou, Guangdong province (China). Divinylbenzene (DVB, 80 %, mixture of isomers) was provided by Alfa Aesar (Tianjin) Chemical Co. Ltd. (China). Ethanol (AR) was obtained from Guanghua Chemical Plant in Guangdong province (China). CTAB was recrystallized by the ethanol-ether mixture (volume ratio 1: 1). APS was recrystallized by water prior to use. Both St and DVB were refined by passing through a column filled with potassium carbonate, silica oxide and aluminum oxide to remove hydroquinone before use. Other reactants were applied as received. Deionized water was used in all the experiments.

### Preparation and polymerization of HIPE

In a 250 mL glass flask, emulsifier CTAB (0.8 wt %, based on monomer) was dissolved in mixed comonomer (St: DVB=90: 10, by volume) with stirring to obtain external phase (oil phase). The internal phase (aqueous phase) was composed of water, ethanol (Water: Ethanol=91: 9, by volume), and initiator APS (1.6 wt %, based on monomer). Different amounts of the aqueous phase was slowly added into the oil phase for about 2 h, further stirred continuously for 5 h at 400 rpm obtaining a stable HIPE. After that, the HIPE was poured into a glass tube and polymerized at 70 °C for 12 h. After drying to constant weight, the porous poly(St-DVB) (PSD) was obtained without further purification. (The products from these were designated as PSD82.5, PSD85.0, PSD87.5, PSD90.0, PSD92.5 and PSD94.0, corresponding to 82.5, 85.0, 87.5, 90.0, 92.5 and 94.0 % of aqueous phase volume in HIPE.)

### Characterizations

The morphology of PSD was observed with a scanning electron microscope (SEM, JSM-6380LV, JEOL Ltd, Japan). The sample surface was gold sputtered prior to observation. The cavity and window sizes were determined by measuring the length of the largest and the smallest cavity or window.

Pore volume and median pore size of the PSD were recorded by mercury intrusion porosimeter using a Micromeritics Autopore IV 9500 porosimeter. Samples were subjected to a pressure cycle from 0.1 psia to 60,000 psia.

The apparent density of PSD was determined by calculating the weight ( $m$ , in gram) and volume ( $V$ , in cubic centimeter) of the PSD cylinders (the cylinder was due to the shape of a glass tube), in which the volume was obtained by measuring the radius ( $r$ , in centimeter) and the height ( $h$ , in centimeter) of the PSD cylinders. The apparent density is calculated according to Eq. (1).

$$\text{Apparent density} = m/V = m/\pi r^2 h \quad (1)$$

The water and toluene absorption values of PSD were determined in a beaker. The samples were weighed ( $m_{\text{dry}}$ , in gram) and immersed in the liquid. The samples were removed, blotted with filter paper and weighed ( $m_{\text{wet}}$ , in gram) every minute for the first 10 min and for longer intervals thereafter. The water and toluene absorption values of PSD (absorption, in cubic centimeter per gram) were calculated using Eqs. (2) and (3), respectively.

$$\text{Water absorption} = (m_{\text{wet}} - m_{\text{dry}})/m_{\text{dry}} \quad (2)$$

$$\text{Toluene absorption} = (m_{\text{wet}} - m_{\text{dry}})/(0.866m_{\text{dry}}) \quad (3)$$

In the Eq. (3), 0.866 is the density (in unit of  $\text{g}/\text{cm}^3$ ) of toluene at room temperature ( $20\text{ }^\circ\text{C}$ ).

The volume of the samples after swelling in the toluene ( $V_{\text{after}}$ ) was also determined by measuring the radius ( $r$ , in centimeter) and the height ( $h$ , in centimeter) of the PSD cylinders. The volume expansion of the samples was calculated using Eq. (4).

$$\text{Volume expansion}(\%) = (V_{\text{after}} - V) / V \times 100 \quad (4)$$

The release of PSD was carried out by immersing it ( $m_{\text{dry}}$ , in gram) in toluene for 24 h. The samples were then removed, blotted with filter paper, and weighed ( $m_0$ , in gram). Afterward, the wetted samples were placed in air at room temperature and weighed ( $m_{\text{rt}}$ , in gram) every 10 min for the first 60 min and then every 30 min for the last 120 min. The release of toluene for PSD (release, in cubic centimeter per gram) was calculated according to Eq. (5).

$$\text{Release} = (m_{\text{rt}} - m_{\text{dry}}) / (0.866m_{\text{dry}}) \quad (5)$$

The compressive modulus of PSD was determined on a universal testing machine. Cylinder samples with height of  $8 \pm 1$  mm and diameters of  $54 \pm 1$  mm were used. Stress–strain curves were obtained at a strain rate of  $0.125\text{ } \%/s$  and room temperature until  $75\text{ } \%$  deformation was reached.

## Results and discussions

### Preparation and polymerization of HIPE

A series of HIPEs with internal-phase contents varied from 82.5 to 94 % was prepared and polymerized using CTAB as emulsifier and APS as initiator. When the internal-phase content was below 82.5 %, the water and oil phases were very well emulsified under stirring conditions. However, the emulsion was separated into two phases during the polymerization when stirring was not performed. Thus, polymerization did not occur at  $70\text{ }^\circ\text{C}$  even for 12 h because no initiator was presented in the oil phase. Meanwhile, the viscosity and the stability of the emulsion increased with increased volume fraction of the water phase. In this case, phase separation did not occur during the polymerization, and polymerization smoothly occurred, resulting in porous polymers (Figs. 1a to h). When the internal-phase content reached 94.0 %, the HIPEs maintained their stability for at least 3 days, and normally polymerized. However, further increased the internal-phase content to 95 % resulting in demulsification because of the increase in the volume of the water phase. The thickness of the continuous phase continuously decreased with increased internal-phase content. The film broke at sufficiently low

thickness, thereby leading to phase separation and the absence of monomer polymerization.

### Microstructure of the polyHIPEs

The SEM images of the PSD samples with internal-phase contents of 82.5–94.0 % are shown in Fig. 1. The SEM images showed that the porous polymers were successfully prepared using the HIPEs as template, and the internal-phase content markedly influenced the microstructure of the polyHIPE solid foams. An interconnected porous structure with cavities, cavity walls, and windows within the cavity walls was observed in the samples when the aqueous phase content was 82.5 to 90.0 %. When the aqueous phase contents were 82.5 and 87.5 %, the cavity sizes ranged from 100 to 300  $\mu\text{m}$ , while the window sizes were in the range of 2  $\mu\text{m}$  to 10  $\mu\text{m}$ , and thick cavity walls were observed. As the increase of internal-phase content, more open and porous structure monoliths were found, the cavity sizes became smaller and smaller, while the windows sizes became bigger and bigger, thus, the cavity wall became thinner and thinner. When the internal phase content was 94 %, no cavity was seen in the SEM image. In addition, the interconnected structures in the polyHIPE were more and more obvious. The porous polymer with 94.0 % internal-phase content exhibited the thinnest cavity wall, while the polyHIPE with 90.0 % internal-phase content displayed the most uniform interconnected structure.

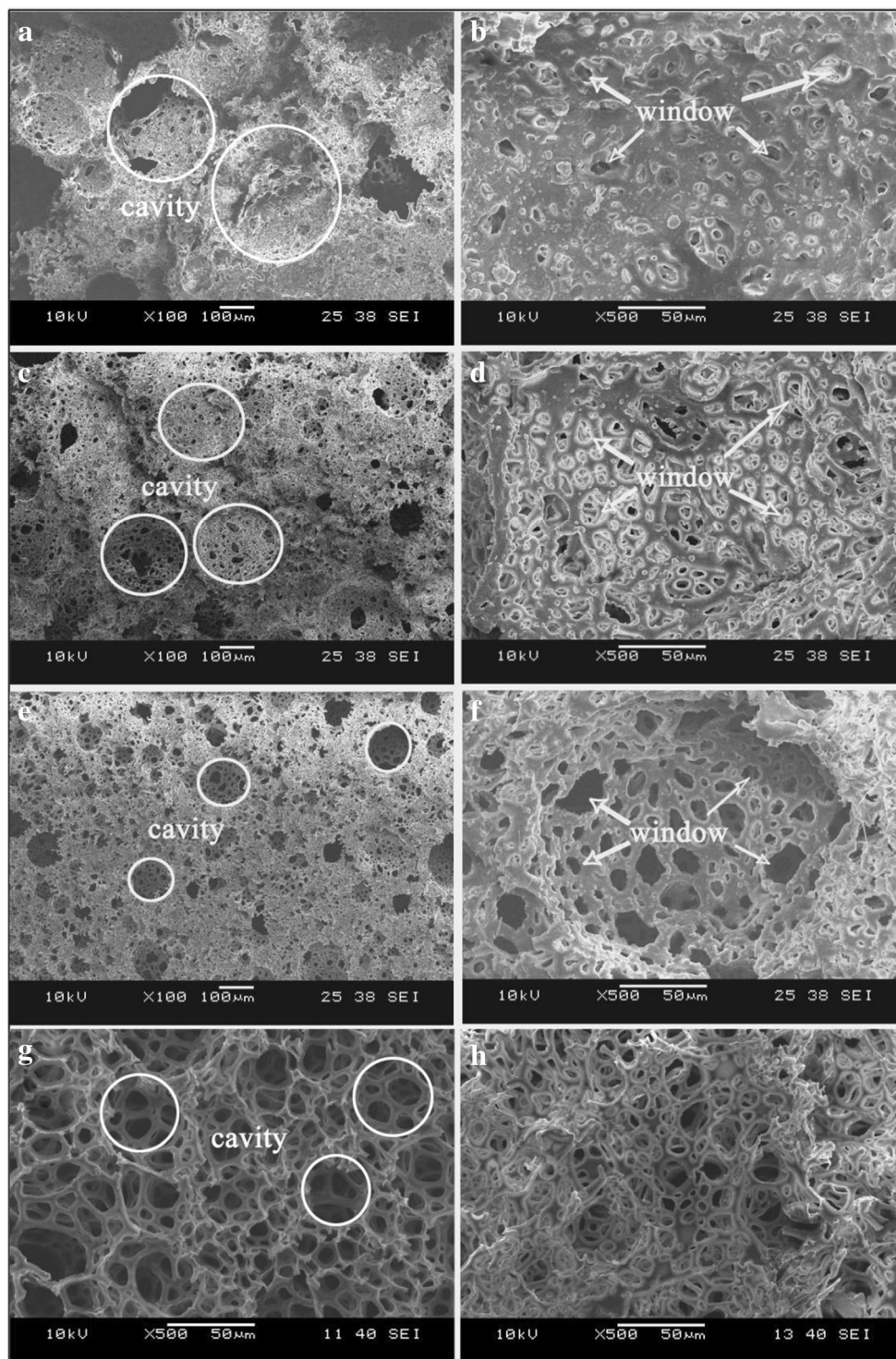
Table 1 showed that the apparent densities of the porous polymer were very low ( $<0.25\text{ g}/\text{cm}^3$ ) and decreased with the increase of the internal-phase contents, however, pore volume and porosity of the porous polymers increased with the internal-phase contents except for the sample with 94 % internal-phase content. The median pore diameters of the porous polymer were almost the same except for the sample with 90 % internal-phase content. Because median pore sizes are the result of average cavity size and windows size, larger cavity size and smaller windows size may lead to almost the same median pore size.

### Absorption of the polyHIPEs

The water absorption curves of the PSD samples are illustrated in Fig. 2a and the balanced water absorption values are listed in Table 2. The water absorption value increased rapidly with the increase of internal-phase content, and water absorption reached equilibrium within about 3 min. This phenomenon was due to the increased pore volume. PSD94.0 exhibited the highest water absorption value at a plateau of  $11.65\text{ cm}^3/\text{g}$ . By contrast, PSD82.5 had the lowest water absorption value of only  $2.37\text{ cm}^3/\text{g}$ . This low absorption reflected the low pore volume of the PSD samples. Water absorption in our experiments is higher than the value in literature [30]. In our case, the higher pore volume was obtained with higher internal



**Fig. 1** SEM images of PSD with various internal-phase content: **(a** and **b)** 82.5 %; **(c** and **d)** 85.0 %; **(e** and **f)** 87.5 %; **(g)** 90.0 %; **(h)** 94.0 %



phase content. Generally, the poly(Styrene-co-DVB) is hydrophobic, the PSD after extraction is also hydrophobic. However, before extraction, the PSD was hydrophilic due to the existence of emulsifier. The PSDs in our experiments were not extracted, thus more amounts of water were absorbed.

The variations in toluene absorption values for different time of the porous polymer foams with various

internal-phase contents are shown in Fig. 2b and Table 2. A rapid increase in the toluene absorption curve was observed during the first 5 min, and then a plateau was reached. PSD94.0 had the highest toluene absorption value ( $21.64 \text{ cm}^3/\text{g}$ ), whereas PSD82.5 had the lowest toluene absorption value (only  $6.74 \text{ cm}^3/\text{g}$ ). The toluene absorption value significantly increased

**Table 1** Properties of the porous polymer

Samples	Density (g/cm <sup>3</sup> )	Total intrusion volume (mL/g)	Median pore diameter (μm)	Porosity (%)
PSD82.5	0.248	6.0	18.0	79.7
PSD85.0	0.120	7.4	16.8	84.3
PSD87.5	0.095	9.7	20.7	87.0
PSD90.0	0.072	13.4	6.5	97.4
PSD94.0	0.058	11.9	18.0	73.9

with increased aqueous phase contents, because of the increased pore volume.

Moreover, the toluene absorption value was clearly higher than the water absorption value because of the swelling behavior of the polymer after immersion in toluene. The volume of the porous polymers enlarged to about twice their original size after swelling in toluene (ref Table 2). However, the weight changes were minimal after the swollen PSD dried. This results enabled the toluene absorption value to become about twice the water absorption value.

Absorption kinetics

Absorption models were used to investigate the absorption kinetics according to the literature [31, 32] in order to understand the absorption behaviors of PSD. The pseudo-first-order equation is described as follows:

$$\frac{dQ_t}{dt} = k_1(Q_{eq} - Q_t) \tag{6}$$

Where  $Q_{eq}$  and  $Q_t$  (millimole per gram) are the amounts of water and toluene absorbed at the equilibrium time and measurement time (minute), respectively; and  $k_1$  is the pseudo-first-order rate constant of absorption (per minute), which

indicates the water and toluene absorption speed. After definite integration by applying the initial conditions  $Q_t=0$  at  $t=0$ , Eq. (6) becomes:

$$\ln(Q_{eq} - Q_t) = \ln - k_1 t \tag{7}$$

The pseudo-second-order equation is described as follows:

$$\frac{dQ_t}{dt} = k_2(Q_{eq} - Q_t)^2 \tag{8}$$

$k_2$  is the pseudo-second-order rate constant of absorption (cubic centimetres per gram per minute), which also indicates the water and toluene absorption speed. The equation shows the dependence of the absorption value of the sorbate on time. If the equilibrium absorption values of the PSD rate constant  $k_2$  is known, then the absorption value of PSD at any time can be calculated.

Through integrating this equation by applying the initial conditions  $Q_t=0$  at  $t=0$  and  $Q_t=Q_t$  at  $t=t$ , Eq. (8) becomes:

$$\frac{t}{Q_t} = \left( \frac{1}{k_2 Q_{eq}^2} \right) + \frac{t}{Q_{eq}} \tag{9}$$

Based on Eq. (7), the linear plots of  $\ln(Q_{eq}-Q_t)$  versus  $t$  can be drawn and the slope value is  $k_1$ . Accordingly, the correlation coefficients with pseudo-first-order kinetics were found to be only 0.6577 (Fig. 3a) and 0.4732 (Fig. 3c) for water and toluene absorption, respectively. Thus, the pseudo-first-order kinetics was not applicable to absorption behavior of PSD. However, these absorption behaviors can be well described by the pseudo-second-order equations in which the correlation coefficients for all samples were >0.998 (Figs. 3b and d) for water and toluene absorption. This high

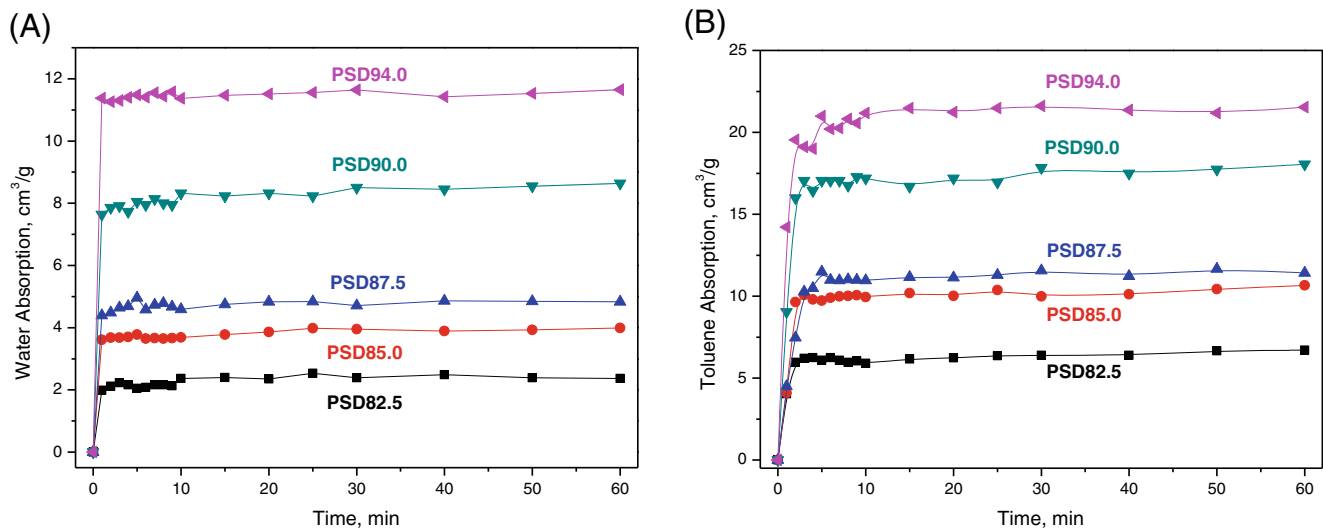


**Fig. 2** Water (a) and toluene (b) absorption curves of PSDs with various internal-phase contents

**Table 2** Absorption of the porous polymer

Samples	Balanced water absorption ( $\text{cm}^3/\text{g}$ )	Balanced toluene absorption ( $\text{cm}^3/\text{g}$ )	Volume expansion in toluene (%)
PSD82.5	2.37	6.74	97.1
PSD85.0	3.89	10.11	90.9
PSD87.5	4.86	11.67	105.3
PSD90.0	8.45	17.74	88.0
PSD94.0	11.65	21.64	95.6

correlation coefficient suggested that the water and toluene absorption values of PSD can be well represented by the pseudo-second-order model.

### Release behavior and kinetics

After immersing the porous polymers in water (or toluene) for 24 h, they were saturated with water (or toluene), and their

release behaviors within 3 h were investigated at room temperature. The results (Fig. 4) indicated that the water and toluene contents of PSDs decreased continuously during the release period, and a linear relationship was found. The data were fitted to a straight line, and the parameters of the fit curves are listed in Table 3. For example, the toluene release rates ( $k_{r2}$ ) of the PSD82.5, PSD85.0, PSD87.5, PSD90.0, and PSD94.0 were 0.018, 0.022, 0.046, 0.081, and  $0.122 \text{ cm}^3 \cdot \text{g}^{-1} \cdot \text{min}^{-1}$ , respectively. These data showed increasing trends with increased internal-phase content because of the increased pore volume of the PSD. In addition, all data fitted well, as confirmed by the fitting correlation coefficient values ( $R_r^2$ ). Larger pore volumes and pore sizes of the sample enabled easier toluene diffusion from the sample. After 180 min, the toluene in the PSD samples with lower internal-phase content almost completely released, whereas in the PSD samples with higher internal-phase contents, some toluene molecules still remained due to the limited release time. The PSDs exhibited slower release for water than

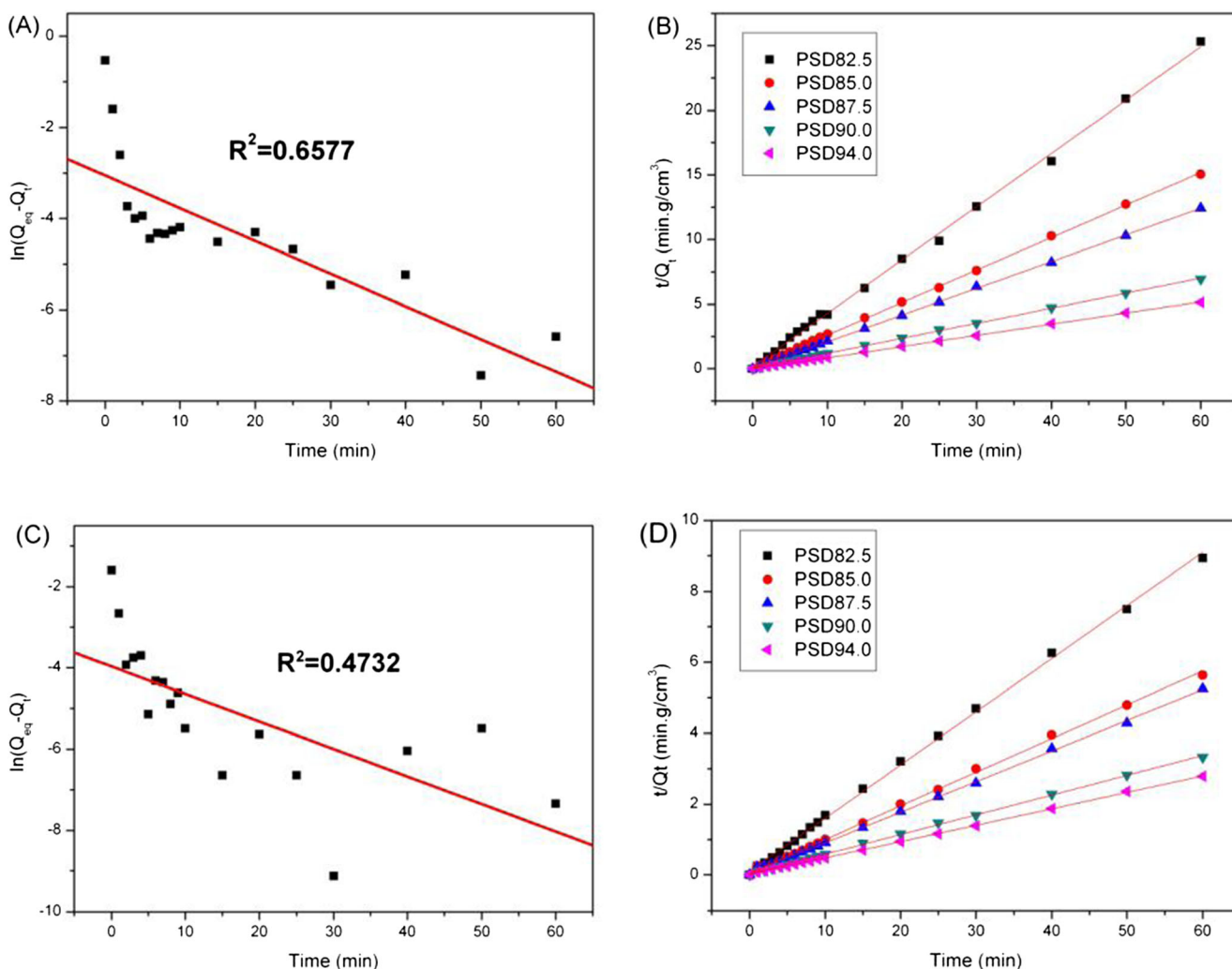


**Fig. 3** Plots of first (a and c) and second (b and d)-order rates of water (a and b) and toluene (c and d) absorption for PSD adsorbent

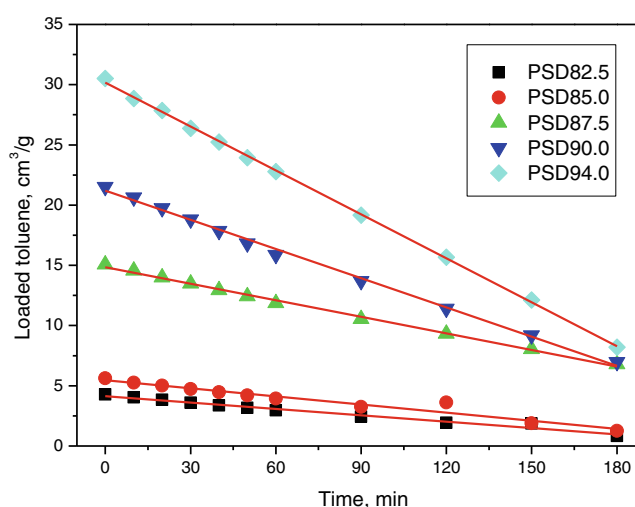
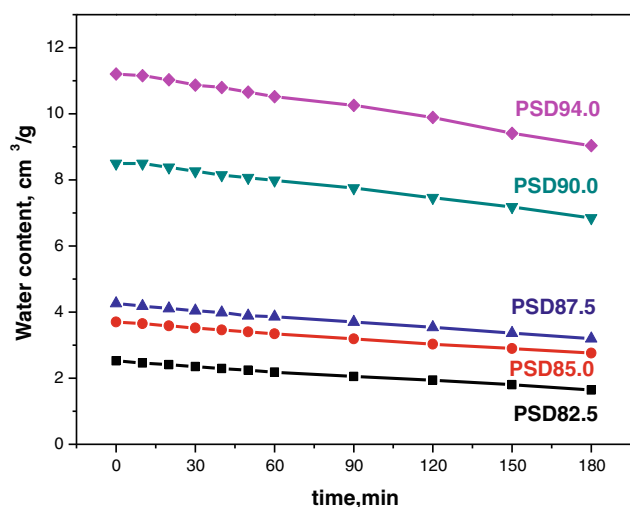


Fig. 4 Water and toluene delivery curves of PSDs with various internal-phase contents

toluene due to their hydrophilicity resulting from the existence of emulsifier CTAB.

Release models were used to investigate the release kinetics of the PSD. The pseudo-zero<sup>th</sup>-order release model equation is described as follows:

$$dQ_t/dt = k_r \tag{10}$$

where  $Q_t$  is the amount of water and toluene released at the measurement time (minute), and  $k_r$  is the pseudo-zero<sup>th</sup>-order rate constant of release (milliliter per gram per minute). After integration by applying the initial condition of  $Q_t=Q_0$  at  $t=0$ , the above equation becomes:

$$Q_t = Q_0 + k_r t \tag{11}$$

Based on Eq. (10), a linear plot of  $Q_t$  versus  $t$  can be drawn (see Fig. 4), and the slope value is  $k_r$  (a negative value, meaning the release of water (or toluene)). The water and toluene release kinetics of the porous polymer were described very well by a pseudo-zero<sup>th</sup>-order kinetic model, which is in contrast to the pseudo-second-order kinetic model as proposed for the corresponding absorption behavior.

Table 3 Parameters for water and toluene release

	PSD82.5	PSD85.0	PSD87.5	PSD90.0	PSD94.0
$k_{r1}$	-0.005	-0.005	-0.006	-0.009	-0.012
$R_{r1}^2$	0.9965	0.9968	0.9960	0.9968	0.9960
$k_{r2}$	-0.018	-0.022	-0.046	-0.081	-0.122
$R_{r2}^2$	0.9763	0.9466	0.9965	0.9965	0.9994

$k_{r1}$  and  $k_{r2}$  are release rates for water and toluene absorption of the PSD

### Compression modulus

The PSD samples were subjected to compression determination, and the compressive stress–strain curves are illustrated in Fig. 5. All porous polymers had typical three-stage stress–strain curves, i.e., a linear stress–strain region, a stress plateau region, and a densification region showing a steep increase in stress. As shown in Fig. 5, the ratio of aqueous to oil phases significantly influenced the Young’s modulus. Increasing internal-phase content decreased the Young’s modulus of the PSD and the height of the plateau while increasing the length of the plateau region. At 40 % deformation, the stress values of the PSD samples with internal-phase content from 82.5 to 94 % were 1.38, 1.02, 0.66 and 0.31 MPa, respectively. This observation indicated the density and wall thickness of PSD, which coincided with the aforementioned SEM and density measurement results. The porous polymers with higher

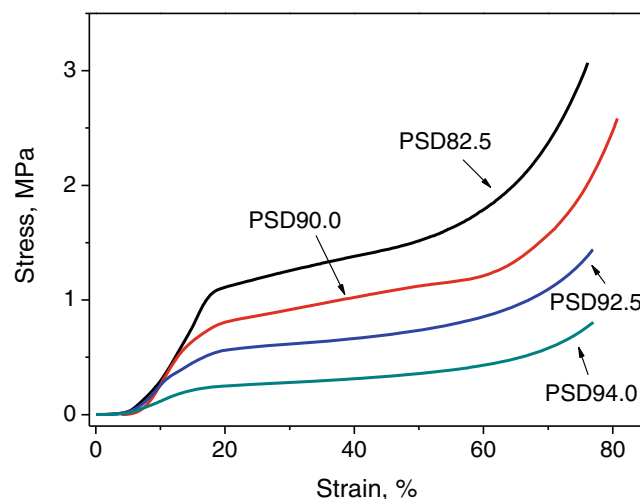


Fig. 5 Compressive stress–strain curves of PSDs with varying internal-phase content



internal-phase contents, larger pore sizes, and thinner intercellular pore walls displayed lower Young's moduli.

## Conclusion

A series of porous polymers was synthesized using HIPE as template and CTAB as a surfactant with different internal-phase contents. The internal-phase contents were found to play a highly important role in the preparation and properties of the porous polymer. Porous polymers were difficult to obtain using the method when the internal-phase content were <82.5 % or >94 %. The increase in the internal-phase content increased the pore volume but decreased the density and compressive strength of the porous polymer. Therefore, the density and pore volume of the polymer can be controlled by the internal-phase content. The internal-phase content also crucially affected the absorption and release of liquids. The water and toluene absorption values significantly increased with increased internal-phase content. The water and toluene absorption values of PSD82.5 were 2.37 and 6.74 cm<sup>3</sup>/g, respectively, but these of PSD94.0 reached 11.65 and 21.64 cm<sup>3</sup>/g, respectively. These results showed that the pore volume of the porous polymer increased with increased internal-phase content. The water and toluene absorption kinetics of the porous polymer were best described by a pseudo-second-order kinetic model, while the release kinetic were described very well by a pseudo-zero<sup>th</sup>-order kinetic model.

**Acknowledgments** We gratefully acknowledge the financial supports from National Natural Science Foundation of China (51263004), Innovation team of Guangxi universities' talent highland, Guangxi Funds for Specially-appointed Expert.

## References

- Sušec M, Ligon SC, Stampfl J, Liska R, Krajnc P (2013) Hierarchically porous materials from layer-by-layer photopolymerization of high internal phase emulsions. *Macromol Rapid Commun* 34:938–943
- Petchwattana N, Covavisaruch S, Pitidhamabhorn D (2013) Influences of water absorption on the properties of foamed poly(vinyl chloride)/rice hull composites. *J Polym Res* 20:172
- Thomas A, Kuhn P, Weber J, Titirici MM, Antonietti M (2009) Porous polymers: enabling solutions for energy applications. *Macromol Rapid Commun* 30:221–236
- Liang C, Li Z, Dai S (2008) Mesoporous carbon materials: synthesis and modification. *Angew Chem Int Ed* 47:3696–3717
- Bae H-S, Haider A, Selim KMK et al (2013) Fabrication of highly porous PMMA electrospun fibers and their application in the removal of phenol and iodine. *J Polym Res* 20:158
- Karesoja M, McKee J, Karjalainen E et al (2013) Mesoporous silica particles grafted with poly(ethyleneoxide-block-N-vinylcaprolactam). *J Polym Sci, Part A: Polym Chem* 51:5012–5020
- Zhang SM, Chen JD, Perchyonok VT (2009) Stability of high internal phase emulsions with sole cationic surfactant and its tailoring morphology of porous polymers based on the emulsions. *Polymer* 50:1723–1731
- Wong LLC, Baiz Villafranca PM, Menner A, Bismarck A (2013) Hierarchical polymerized high internal phase emulsions synthesized from surfactant-stabilized emulsion templates. *Langmuir* 29:5952–5961
- Ho Y-S (2006) Review of second-order models for adsorption systems. *J Hazard Mater* 136:681–689
- Bottcher H, Hallensleben ML, Nuss S, Wurm H (2000) ATRP grafting from silica surface to create first and second generation of grafts. *Polym Bull* 44:223–229
- Liu W, He G, He Z (2011) Polystyrene/magnetite hybrid foams prepared via 60Co  $\gamma$ -ray radiation of high internal phase emulsions. *J Polym Res* 19:9765
- Li C, Yang J, Wang P, Liu J, Yang Q (2009) An efficient solid acid catalyst: Poly-p-styrenesulfonic acid supported on SBA-15 via surface-initiated ATRP. *Microporous Mesoporous Mater* 123: 228–233
- Livshin S, Silverstein MS (2008) Crystallinity and cross-linking in porous polymers synthesized from long side chain monomers through emulsion templating. *Macromolecules* 41:3930–3938
- Qiang Z, Xue J, Cavicchi KA, Vogt BD (2013) Morphology control in mesoporous carbon films using solvent vapor annealing. *Langmuir* 29:3428–3438
- Audouin F, Heise A (2013) Surface-initiated RAFT polymerization of NIPAM from monolithic macroporous polyHIPE. *Eur Polym J* 49: 1073–1079
- Kovacic S, Matsko NB, Jerabek K, Krajnc P, Slugovc C (2013) On the mechanical properties of HIPE templated macroporous poly(dicyclopentadiene) prepared with low surfactant amounts. *J Mater Chem A* 1:487–490
- Mao D, Li T, Liu H et al (2013) Preparation of macroporous polyHIPE foams via radiation-induced polymerization at room temperature. *Colloid Polym Sci* 291:1649–1656
- Ma Q, Liu X, Zhang R, Zhu J, Jiang Y (2013) Synthesis and properties of full bio-based thermosetting resins from rosin acid and soybean oil: the role of rosin acid derivatives. *Green Chem* 15:1300–1310
- Abbasian Z, Moghbeli MR (2010) Open porous emulsion-templated monoliths: effect of the emulsion preparation conditions on the foam microstructure and properties. *J Appl Polym Sci* 116:986–994
- Grande D, Penelle J, Davidson P, Beurroies I, Denoyel R (2011) Functionalized ordered nanoporous polymeric materials: from the synthesis of diblock copolymers to their nanostructuration and their selective degradation. *Microporous Mesoporous Mater* 140:34–39
- Lumelsky Y, Lalush-Michael I, Levenberg S, Silverstein MS (2009) A degradable, porous, emulsion-templated polyacrylate. *J Polym Sci Part A Polym Chem* 47:7043–7053
- Surendran G, Tokumoto MS, dos Santos EP et al (2005) Highly swollen liquid crystals as new reactors for the synthesis of nanomaterials. *Chem Mater* 17:1505–1514
- Azizian S (2004) Kinetic models of sorption: a theoretical analysis. *J Colloid Interface Sci* 276:47–52
- Nghiem QD, Kim DJ, Kim DP (2007) Synthesis of inorganic-organic diblock copolymers as a precursor of ordered mesoporous SiCN ceramic. *Adv Mater* 19:2351–2354
- Ho YS, McKay G (1999) Pseudo-second order model for sorption processes. *Process Biochem* 34:451–465
- Zhao G, Wang J, Li Y, Huang H, Chen X (2012) Reversible immobilization of glucoamylase onto metal-ligand functionalized magnetic FeSBA-15. *Biochem Eng J* 68:159–166



27. Huang X, Hauptmann N, Appelhans D et al (2012) Synthesis of hetero-polymer functionalized nanocarriers by combining surface-initiated ATRP and RAFT polymerization. *Small* 8: 3579–3583
28. Cohen N, Samoocha DC, David D, Silverstein MS (2013) Carbon nanotubes in emulsion-templated porous polymers: polymer nanoparticles, sulfonation, and conductivity. *J Polym Sci, Part A: Polym Chem* 51:4369–4377
29. Zhang S, Chen J (2007) Synthesis of open porous emulsion-templated monoliths using cetyltrimethylammonium bromide. *Polymer* 48:3021–3025
30. Sergienko AY, Tai H, Narkis M, Silverstein MS (2002) Polymerized high internal-phase emulsions: properties and interaction with water. *J Appl Polym Sci* 84:2018–2027
31. Asouhidou DD, Triantafylidis KS, Lazaridis NK et al (2009) Sorption of reactive dyes from aqueous solutions by ordered hexagonal and disordered mesoporous carbons. *Microporous Mesoporous Mater* 117:257–267
32. Chen Z, Zhou L, Zhang F, Yu C, Wei Z (2012) Multicarboxylic hyperbranched polyglycerol modified SBA-15 for the adsorption of cationic dyes and copper ions from aqueous media. *Appl Surf Sci* 258:5291–5298